Springer

KSME

Journal of Mechanical Science and Technology 33 (4) (2019) 1651~1661
www.springerlink.com/content/1738-494x(Print)/1976-3824(Online)
DOI 10.1007/s12206-019-0317-y

Numerical investigation of two-phase flow characteristics in multiphase pump with split vane impellers †

Yi Shi*, Hongwu Zhu, Binbin Yin, Ruiting Xu and Jiate Zhang

College of Mechanical and Transportation Engineering, China University of Petroleum Beijing, 102249, China

(Manuscript Received June 28, 2018; Revised January 2, 2019; Accepted January 4, 2019)

Abstract

Multiphase pump is a cost-effective option for subsea oil and gas field development. The ability to handle different inlet gas volume fractions (GVFs) especially high inlet GVF is critical to the development of pump performance. In this study, the two-phase flow characteristics in normal impeller and split vane impeller at different inlet GVFs were investigated by steady numerical simulations. The gas distribution on blade-to-blade plane and meridional flow channel at different inlet GVFs were analyzed and compared. Gas accumulation area and movement characteristics of the gas-liquid flow in impeller flow passage were also pointed out by unsteady simulations. Experimental results of the pump differential pressure were compared with the numerical simulation results, to validate the accuracy of numerical simulation method. The flow characteristics in pump with modified impeller and its performance at different inlet GVFs were both compared with that of the normal impeller. The steady simulation results of normal impeller in different inlet GVFs show that gas concentrating area in the flow passage increases as inlet GVF grows. The unsteady simulation results indicate that gas pocket firstly occurs on the pressure side of impeller, then moves to the suction side in the middle area of blade and finally transfers to outlet of impeller and disappears. The errors between numerical simulation results and experiment data are below 10 %, which validated the feasibility of the numerical simulation method. Simulation results on the split vane impeller demonstrate that the gas accumulation area in flow passage of the modified impeller is dramatically decreased compared to that of the normal impeller. The performance of the modified impeller is generally better than the normal impeller especially in high inlet GVF conditions.

Keywords: Computational fluid dynamics; Helico-axial pump; High gas volume fraction; Multiphase flow; Split vane impeller

1. Introduction

Multiphase pumps have the advantage to transport the mixture of oil, gas and water by only one pipeline instead of two pipelines which gas and liquid are transported separately. It can intensively reduce the production cost of oil and gas field and extend its lifetime at the same time. For rotodynamic multiphase pump, the fluid is subjected to centrifugal force. Since there is large difference of density between gas and liquid, it easily leads to the separation of gas and liquid. The liquid flows to the shroud of impeller blades while gas gathers at the hub of blade in the flow passage and finally blocks it. Resulting from the decrease of flow area, the axial flow velocity increases and so as the loss of the hydraulic energy. In order to improve the hydraulic performance of multiphase pump, it is necessary to analyze the flow characteristics of gas and liquid, the flow patterns and mechanism of gas-liquid separation. In this way the process of gas accumulation can be better understood. Thus it provides effective guidance for impeller selection and modification to improve the performance of the pumps.

Several studies on gas-liquid distribution in flow passage of multiphase pump have been made in recent years. Zhang et al. [1] investigated the flow patterns of gas-liquid in inlet and flow passage of a three-stage helico-axial multiphase pump by visual experiments. The results of the experiments showed that the flow pattern varies as the inlet GVF increases. It firstly shows a pattern with spreaded gas bubbles in liquid followed by bubbly flow, gas pocket flow and segregated gas flow. Gas mainly concentrates on the suction side of impeller blade. This is also observed in the visual experiments of a one-stage helico-axial multiphase pump carried out by Serena and Bakken [2]. They pointed out that the gas accumulating area would decrease by increasing the rotational speed of the impeller. These studies above were conducted in relatively low inlet GVF conditions which are lower than 30 %. In order to understand the hydrodynamic behavior in flow passage of impeller in high inlet GVF conditions, Faustini and Kenyery [3] made steady numerical simulations on a one-stage pump with high inlet GVFs (60 %, 70 % and 80 %). The gas-liquid flow patterns and effects of inlet GVFs and volume flow rates on the

*Corresponding author. Tel.: +86 15201251687
E-mail address: shiyicup@gmail.com
† Recommended by Associate Editor Donghyun You
© KSME & Springer 2019

distribution of gas around impeller were also analyzed. While the steady numerical simulation results could only show the position of gas pocket, unsteady numerical simulation methods were used to investigate the characteristics of gas pocket movement in impeller flow passage. Suh et al. [4] established an unsteady numerical simulation method to investigate the unsteady characteristics of water volume fraction on meridional plane of the impeller and diffuser in low inlet GVF conditions. It showed that a certain pattern developed as the flow proceeded from the hub to shroud as a function of time and the regional gas volume fraction became larger between the rotating and the static parts.

As for the researches on improving performance of the helico-axial multiphase pumps, modifications on the parameters of impellers are the most concerned. Zhang et al. [5] developed a multi-objective optimal method for characterizing impellers by combining artificial neural network (ANN) with non-dominated sorting genetic algorithm-II (NSGA-II). The main geometric parameters affecting impeller's performance such as impeller shroud inlet angle, impeller shroud outlet angle, half cone angle of the hub and the hub ratio of import were all optimized. It shows that the gas accumulating area on the discharge area of the optimized impeller blade surface decreases significantly and the performance of the compression unit was improved. Kim et al. [6] conducted a design optimization by both the design of experiment (DOE) and numerical analysis. They found that the non-uniform flow components observed on the base model were sharply suppressed and the volume of gas was reduced in the optimized model. There were also several researches focusing on modifying the structure of impeller to improve its performance. Vilagines et al. [7] proposed a concept new type of impeller blade which was called tandem blade. Blades of tandem design comprising vanes made up of one or more profiles or blades were used in the invention. Each group of blades comprised two blades, the main blade and auxiliary blade. They were arranged in relation to each other to optimize the compression of a multiphase fluid and to re-mix the gas and liquid phase. But there are not any studies on the two-phase flow characteristics in flow passage or performance of the new impeller. Similarly, Serena and Bakken [8] suggested that additional gaps on the impeller blades should be made to break gas pocket in the flow passage of the impeller. Morrison et al. [9, 10] developed a split vane impeller pump (SVIP). It was a multi-vane electrical submersible pump (ESP) and the purpose was to transfer homogenized flow and finer bubbles to delay the surging and gas lock condition until higher GVF occurred. And the gas handling capacity of typical multiphase ESPs can be finally increased up to 70 %. The flow behavior in the diffuser sections of the pump were studied and gas concentrations within the stages were analyzed by utilizing the electrical resistance tomography (ERT) system on the first two stages of a three-stage SVIP pump.

In summary, although some new impeller blade profiles have been proposed to improve the performance of helico-axial multiphase pump in previous researches, the flow characteristics such as the gas concentrations, velocity distributions in the flow passage for the modified impeller are neither clear nor discussed in details especially in high inlet GVF conditions. This paper firstly carries out steady numerical simulations of an impeller at different GVFs range from 10 % to 90 %. Aiming to analyze the gas distribution pattern in flow passage and determine the exact gas accumulating area. Then the transient numerical simulations are made to study the characteristics of gas movement in flow passage in high inlet GVF conditions. Based on the numerical simulations results, a modified impeller is developed by splitting the blade to generate a small flow passage where gas is most likely to gather. The modified impeller is different from the structure of that developed by Morrison which mentioned above. Because the impellers in electrical submersible pumps are radial or semi-axial, while they are axial in helicon-axial pumps. But it could also be called split vane impeller. It is designed to improve the performance of multiphase pumps with high inlet GVFs. The performance of a one-stage pump with split vane impeller is compared with normal impeller at different inlet GVF conditions. The results of this paper will be a base for further study on the mechanism of gas pocket and measures to diminish gas pocket in the flow passage with high inlet GVFs, which are significant challenges for such pumps.

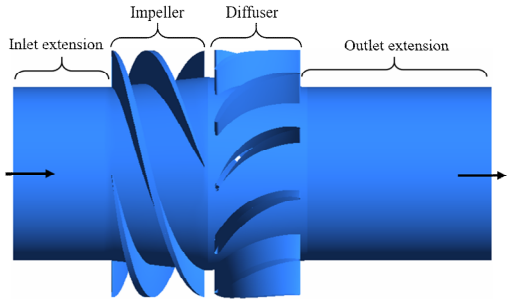

Fig. 1. Geometry model of one-stage pump.

2. Geometry model

The research object in this study is a one-stage pump. It contains an impeller, a diffuser, the inlet and outlet extended regions. The overall geometry of the model is shown in Fig. 1. The inlet and outlet extended regions are defined sufficient far from the impeller and diffuser to diminish its influence on working conditions. The inlet extended region is the same length of the impeller while the outlet extended region is twice length of that one. The impeller has 4 blades, the diffuser has 11 blades and their geometry are created by the program of BladeGen16.0. The shroud diameters of impeller and diffuser are both 135 mm. The designed volume flow rate is 100 m^3/h and the rotational speed of the impeller is 4500 rpm. All parameters of the compression unit are the same as that of the test pump prototype installed on the experimental bench.

3. Computational methodology

3.1 Computational model

The numerical simulation was conducted using commercial CFD software ANSYS CFX16.0. It is recognized for its outstanding accuracy, robustness and wide range of speeds with rotating machinery such as pumps, fans, compressors, and gas and hydraulic turbines. The three-dimensional Reynolds-averaged Navier-Stokes equation was used for turbulent flow analysis in order to examine the characteristics of the internal flow field. There are some turbulence models available in the numerical tools [11]. The choice of turbulence model is always an important step in CFD simulation since the multiphase flow is complicated. The flow medium in the pump are water and ideal gas, which are considered as continuous phase and dispersed phase, respectively. Considering the mixture of gas and liquid is easy to separate in the rotational flow passage of the impeller. The *SST k-w* model is used for water as it results in relatively good solutions to the flow with a large area of separation while the dispersed-phase zero equation model is used for ideal gas [12]. Eulerian-Eulerian multiphase flow model is used in this numerical investigation [13-15]. Assume that gas-liquid flow is homogeneous at the inlet of the impeller [16]. There is no mass transfer between the two phases and no cavitation occurs. Since the isothermal condition is applied to the fluid flow domain in this study, the conservation equation of energy can be neglected. The continuity and momentum equation for turbulent flow are defined as follows:

Continuity equation:

$$\frac{\partial \rho}{\partial t} + \nabla(\rho v) = 0 \tag{1}$$

where ρ and v are liquid density and velocity vector.

Momentum transfer equation:

$$\frac{\partial(\rho v)}{\partial t} + \nabla(\rho v v) = -\nabla P + \nabla(\tau) + \rho g + F_i \tag{2}$$

where τ is the stress-strain tensor, g is the gravity acceleration vector, F_i is the interphase force. For fluid flow in helico-axial pumps in the present study, F_i is a resultant force associated with drag, lift, virtual mass turbulent dispersion [17]. The Basset and Magnus force are not considered as they are negligibly small compared to the other forces since the particle size is small and the rotation of the gas bubbles is assumed negligible.

Equation of gas volume fraction and water volume fraction:

$$\alpha_g + \alpha_l = 1 \tag{3}$$

where α_g and α_l represent the gas volume fraction and liquid volume fraction respectively.

Ideal gas state equation is:

$$p_1 Q_{g1} = p_2 Q_{g2} = const \tag{4}$$

where p_1 and p_2 represent the absolute pressure of the pump inlet and absolute pressure in gas pipeline. Q_{g1} and Q_{g2} represent the gas volume rate of pump inlet and the gas pipeline.

The resultant interphase force acting on the two phases can be expressed as follows:

$$F_i = F_i^D + F_i^L + F_i^A \tag{5}$$

where F_i^D represents the drag force per unit volume. It is given by Noroozi and Hashemabadi [18]:

$$F_i^D = \frac{3}{8}\frac{C_D}{r_g}\rho_l(v_l - v_g)\left|v_l - v_g\right| \tag{6}$$

where C_D is the drag coefficient given by Tabib and Schwarz [19], Re is the Reynolds number:

$$C_D = \begin{cases} 24\left(1 + 0.15Re^{0.687}\right)/Re & Re \le 1000 \\ 0.44 & Re > 1000 \end{cases} \tag{7}$$

$$Re = 2\rho_l \frac{\left|v_l - v_g\right|}{\mu_l} r_g \,. \tag{8}$$

F_i^A represents the virtual mass force per unit volume. It can be described by the following expression [20]:

$$F_i^A = \rho_l C_A \alpha_g a_A \tag{9}$$

where the value of $C_A = 0.5$ has been commonly used for spherical bubbles.

F_i^L represents the lift force per unit volume. It can be described as:

$$F_i^L = \rho_l C_L \alpha_g (v_g - v_l) \times (\nabla \times v_l) \tag{10}$$

where the lift coefficient $C_L = 0.5$, which is the most common value for bubbly flow [21].

3.2 Solving method and boundary conditions

Boundary conditions are defined for all the calculations carried out. At the inlet of computational domain, the mass flow was given as non-swirl flow. While at the outlet, an averaged static pressure is given. All the wall boundaries including the pressure and suction surfaces, the hub and shroud walls of impeller were set as non-slip wall conditions. The interaction between rotating impeller and stationary diffuser was represented by considering the transient sliding interface as attaching boundary conditions. At this interaction, the mass and momentum of all flows were conserved with every pitch change. The governing equations were discretized by finite

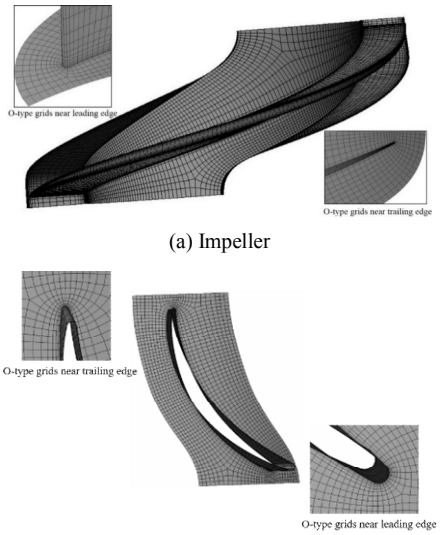

(a) Impeller

(b) Diffuser

Fig. 2. Grids of one flow passage.

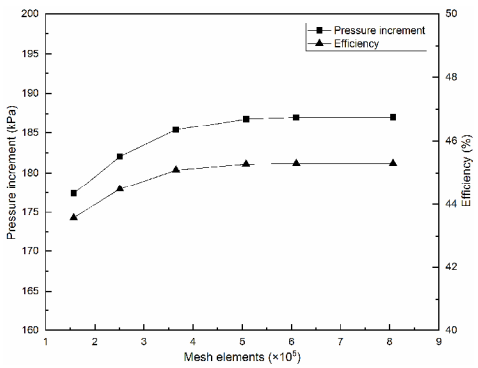

Fig. 3. Grid independence test.

volume method. First-order upwind scheme was selected for the GVF term to calculate the advection terms while second-order upwind scheme was selected for other terms such as momentum. RMS was selected to assess when convergence was reached and the residual level was set as 10^{-6}. The max iteration was set as 3000.

3.3 Grid independence test

Structured grids were adopted for the entire flow fields to obtain high mesh quality. The ANSYS CFD code Turbo-Grid was used to create the whole flow passage grids of impeller and diffuser. It is an integral part of the CFX and it can create high-quality hexahedral mesh while preserving the underlying geometry, allowing for accurate and fast CFD analysis. Fig. 2 shows the grids of one flow passage on impeller and diffuser. The O-type girds near the leading and trailing edge are also presented to show the details. The grids of the inlet and the outlet extended regions were generated by ICEM CFD 16.0.

In order to save calculating time and improve the accuracy

Table 1. Experimental conditions and uncertainties of the measured parameters.

Parameter	Series	Range	Uncertainties
Liquid flowrate	LDBE-80 electromagnetic flowmeter	5-160 m^3/h	± 0.5 %
Gauge pressure	1151 pressure transmitters	0-1.6 MPa; -0.1-1.6 MPa	± 0.1 %
Gas flowrate	LWQ-50 turbine flow meter	5-100 m^3/h	± 1.5 %
Torque	YH 502	0-500 Nm	± 0.5 %

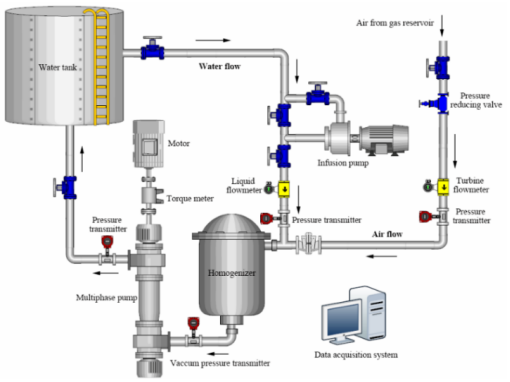

Fig. 4. Schematic diagram of the experimental bench.

of computation, a grid-dependence test was performed with various numbers of grids for the impeller. The initial number of mesh elements of the impeller is about 150000. Then it is increased by an increment of 100000. The efficiency and pressure increment of the one-stage pump are calculated according to the simulation results. The relationships between the pump performance and the number of impeller grids are shown in Fig. 3. The differential pressure and efficiency of the single-stage impeller both increase gradually as the mesh elements increase. And then they tend to be stable when the mesh elements exceed 500000, which means there is not big difference of pump performance even though the mesh elements continue to increase. Then the final mesh elements number of impeller and diffuser are 507760 and 536.877, respectively. The average value of y^+ on impeller blade surface is 17.9, which means the first grid layer can be sufficiently fine to meet the standard wall function requirement($y^+ < 100$). The mesh elements of inlet and outlet extended regions are 46800 and 93600. Total number of mesh elements of the whole model is 1185037.

4. Validation of the numerical simulation method

To validate the numerical simulation method, a performance evaluation was implemented through an experiment on the base model. The schematic diagram of the experimental bench is shown in Fig. 4. The test bench and experiment are based on the standard GB/T3216-2005, which is for hydraulic performance acceptance test of rotodynamic pump. The man-

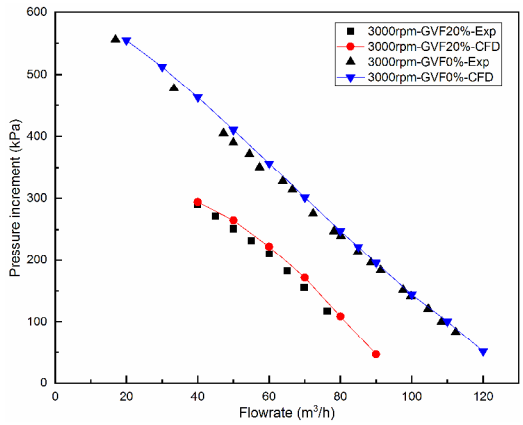

Fig. 5. Comparison of experimental data and simulation results of three-stage pump performance in single-phase flow and gas-liquid.

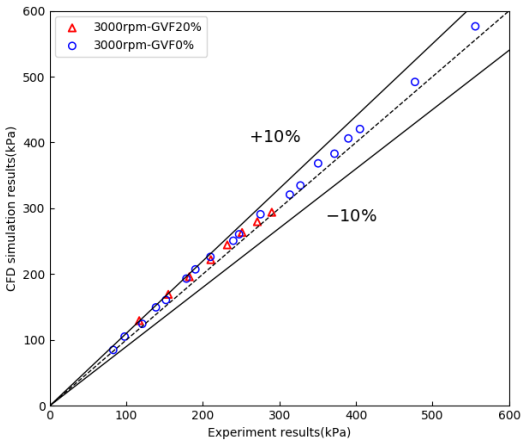

Fig. 6. Error analysis between simulation results and experimental results of the three-stage pump performance.

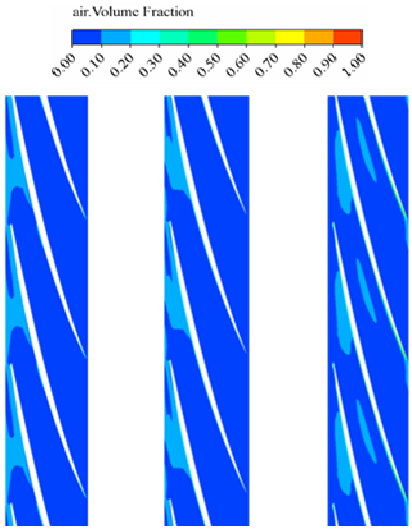

(a) 10 % span-wise (b) 50 % span-wise (c) 90 % span-wise

Fig. 7. Gas distribution on blade-to-blade plane (inlet GVF is10 %).

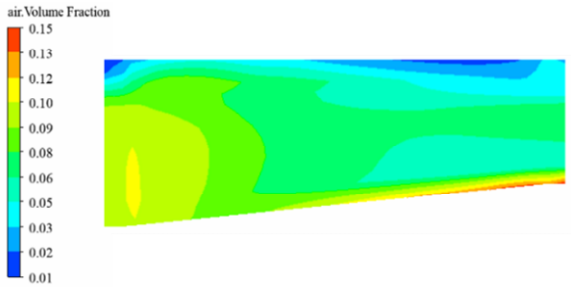

Fig. 8. Gas distribution in meridional flow channel (inlet GVF is 10 %).

ufactured prototype of the base model was installed. A three-stage helico-axial multiphase pump was installed in the experimental system. The rotational speed of the pump was controlled by an inverter. The pump outlet valve was installed to regulate the volume flowrates so that the pressure performance curves could be produced. A torque meter was installed between the couplings to measure the torque of pump shaft. As for the multiphase flow performance evaluation, the facility was supplemented by adding a setup for gas injection. Gas is supplied by a compressor from an air reservoir. The volume of the air reservoir is 2 m^3 with the preset pressure 0.8 MPa. The start-up and shut down of compressor is automatically determined according to the pressure in the air reservoir, which makes sure the gas pressure is stable. A flow homogenizer is installed at the upstream of pump inlet. Water and gas flow into the homogenizer through a tee pipe and mixed sufficiently in the homogenizer [22]. Thus, the two-phase flow entering into the pump could be considered as homogenous.

Table 1 shows the uncertainties of measurement parameters from the devices used in experiment. The uncertainty of the liquid flowmeter is ±0.5 %. The uncertainty of the gauge pressure transmitters is ±0.1 %. The uncertainty of the gas flowmeter is ±1.5 %. The uncertainty of the torque meter is ±0.5 %.

Simulation results of the three-stage helico-axial multiphase pump were compared with experimental results with the same geometry parameters and working conditions. Fig. 5 shows the comparison of experimental data and simulation results in both single-phase flow and gas-liquid flow conditions. More experimental data at different rotational speeds and inlet GVFs are shown in Ref. [15]. The rotational speed is 3000 rpm. For single-phase flow, the simulation results are generally higher than the experiment data, but the difference is not apparent. For the gas-liquid flow, the simulation results fit well with the experiment data at low flowrate and then the simulation results are higher than the experimental data. The difference increases as the flowrate grows. In Fig. 6, the horizontal and vertical coordinates stand for experimental and simulation results, respectively. As can be seen, numerical simulation predicts the three-stage pressure increment with an error below 10 % compared with the experimental results. The deviation may be due to that the flow conditions were relatively ideal to the real flow and it is hard to consider the leakage loss in numerical simulations, which causes the simulation results are a little higher than the experimental results. But the error is within the error ranges and is acceptable.

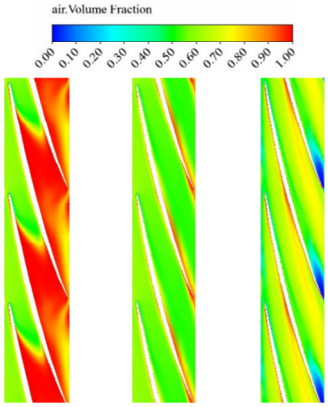

(a) 10 % span-wise (b) 50 % span-wise (c) 90 % span-wise

Fig. 9. Gas distribution on blade-to-blade plane (inlet GVF is 60 %).

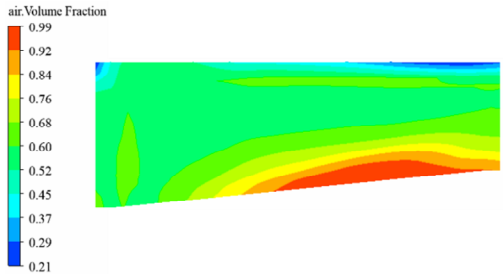

Fig. 10. Gas distribution in meridional flow channel (inlet GVF is 60 %).

5. Results and discussion

5.1 Flow characteristics in normal impeller

The flow characteristics in impeller of the one-stage pump at different inlet GVFs range from 10 % to 90 % are all studied by numerical simulations. The following parts show the flow characteristics in normal impeller with relative low and high inlet GVFs.

Firstly, gas distribution on different blade spans of the cascade planes are shown in Fig. 7 when the inlet GVF is 10 %. The 10 % span-wise is near the impeller hub while the 90 % span-wise is close to the impeller shroud. The variation of gas volume fraction from hub to shroud on the impellers is not apparent. Gas mainly concentrated on the suction side near hub of impeller on the blade-to-blade plane. Fig. 8 shows the gas distribution in the meridional flow channel of the impeller. High gas volume fraction occurs at hub near the outlet of the impeller. The maximum GVF there is about 15 %. Gas volume fraction decreases from hub to shroud along the radial direction and impeller shroud is occupied by almost pure water.

When inlet GVF increases to 60 %, the characteristic of gas distribution is different from that of low inlet GVF. Fig. 9 shows that most area of flow passage are full of gas at the 10 % span-wise. While the gas concentrating area decreases at the 90 % span-wise. Gas only concentrates on suction side of the impeller near the middle position of the flow passage. Water mainly concentrates at the outlet of blade on the pressure side at the 90 % span-wise. Because of the dif-ference between gas and water density, the effect of different centrifugal forces focused on gas and water becomes more obvious at high inlet GVF conditions. Gas distribution in the meridional flow channel of the impeller is shown in Fig. 10. Gas concentrating area mainly occurs at hub. The maximum GVF there can be as high as 100 %. The area is larger than that of the low inlet GVF presented above. It mainly distributes from the central area of the flow passage to the outlet of impeller. The gas concentrating area near hub expands as the inlet GVF increases. Meanwhile, water just occupies a small part of area on impeller shroud. The trajectory of an isolated gas bubble in meridional flow plane is shown in Fig. 11. To simplify the analysis of gas bubble movement, the gas bubbles are considered spheroidal. W_s is the velocity along the flow direction from impeller inlet to outlet. Since there is a big difference between gas and liquid density, the centrifugal force focuses on water is larger than that of gas bubbles. Thus, there is a relative velocity W_n in radial direction. The absolute velocity is W, which points to impeller hub. That is why gas mostly concentrated at impeller hub. The conclusion fits well with the results in Zhang's study [23].

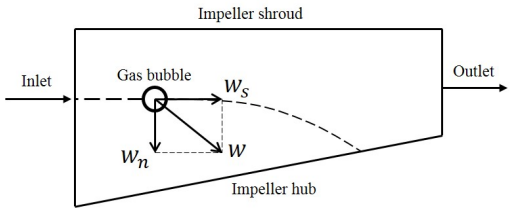

Fig. 11. The trajectory of an isolated gas bubble in meridional flow channel.

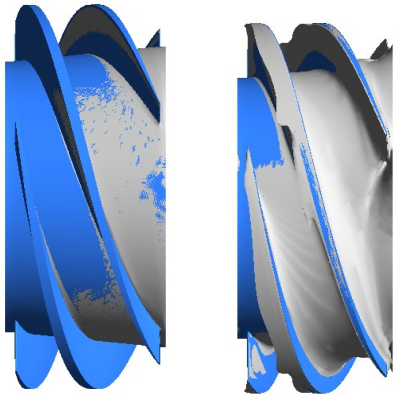

(a) Inlet GVF is 10 % (b) Inlet GVF is 60 %

Fig. 12. The iso-surface gas volume fraction in the three-dimensional flow passage.

In order to show the gas concentrating area in the flow passage of the impeller more accurately and directly, the iso-surface gas volume fraction distribution in three-dimensional flow passage in both low and high inlet GVF conditions are shown in Fig. 12. The value of the iso-surface gas volume fraction is 85 %, which means the gas volume fraction in grey

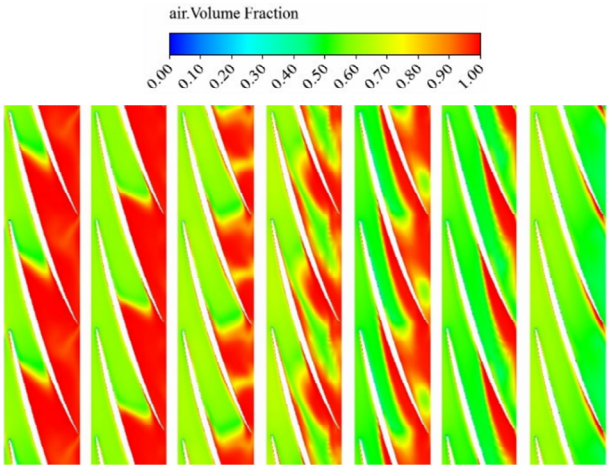

(a) T_0 (b) T_0+t (c) T_0+2t (d) T_0+4t (e) T_0+8t (f) T_0+10t (g) T_0+12t

Fig. 13. The movement of high gas volume fraction area at 10 % span-wise of blade-to-blade plane.

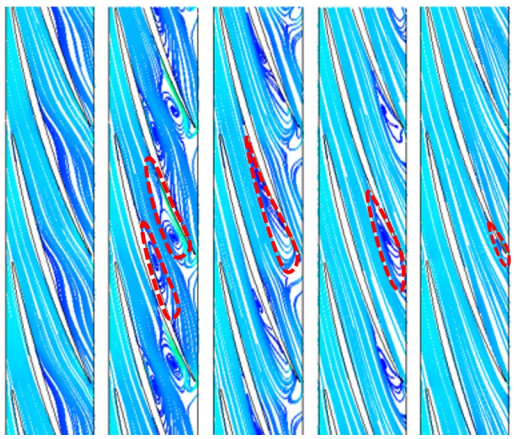

Fig. 14. The streamline of gas velocity at 10 % span-wise of blade-to-blade plane.

areas in Fig. 12 is 85 %. It mainly occurs at hub near the export and suction side of the impeller when the inlet GVF is low, while it occurs both on the suction and pressure side in high inlet GVF condition and the majority area of flow passage is full of gas, which finally leads to larger hydraulic losses. Then the performance of impeller is dramatically degraded. Therefore, suppressing or diminishing the gas concentration area contributes to improve the performance of multiphase pump.

To investigate the movement characteristics of the gas-liquid flow in high inlet GVF condition, unsteady simulations were conducted based on the above steady simulation results on a one-stage pump. In the unsteady simulation, the inlet volume flow rate is 100 m^3/h, rotational speed is 4500 rpm and inlet GVF is 60 %. The impeller rotates for 1° in each time step and the time step is 3.70e-5 s based on the typical cell size and the characteristic flow velocity. The result is saved for further analysis once impeller rotates for every 15°. Gas distribution on the 10 % span-wise of the blade-to-blade plane of the impeller at different stable periods is shown separately in Fig. 13. T_0 is the time at the beginning of a certain stable period during the whole simulation time, and t is the time when the impeller rotates for one circle. Fig 14 shows the streamline of gas velocity at 10 % span-wise of blade-to-blade plane. Figs. 14(a)-(e) are corresponding to Figs. 13(c)-(g), respectively. The color shade represents different values of gas velocity. The value of gas velocity is zero in the area with dark color, which means there are gas gathering there. Figs. 13 and 14 show that high gas concentrating area firstly occurs on most part of the flow passage especially on the pressure side. Then gas bubbles gradually move to the impeller outlet along the pressure side. Most of them move to the suction side because vortex occurs near the impeller outlet. As the vortex becomes larger, all the gas bubbles gather on suction side of impeller. While the vortex decreases, the gas bubbles generally move to impeller outlet along the suction side. The red circles with dotted line in Fig. 14 show the gas vortex in flow passage. They clearly show the gas concentrating area and the movement of gas bubbles. It could also be concluded that the process of gas transportation from inlet to the outlet of impeller was not consistent. This phenomenon can only be captured by transient numerical simulations.

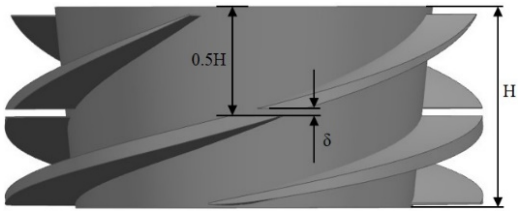

Fig. 15. Three-dimension model of the modified impeller.

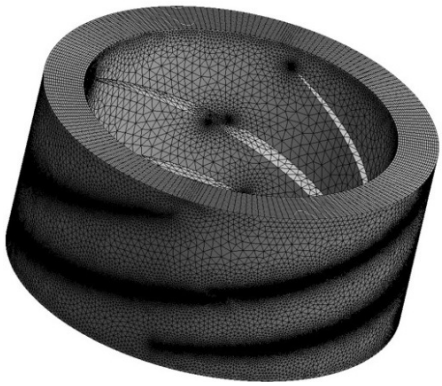

Fig. 16. Mesh of the modified impeller.

5.2 Flow characteristics in split vane impeller

An effective way to improve the performance of the impeller with high inlet GVFs is to re-mix the separated gas and liquid in the flow passage. A modified impeller with split vane was developed. According to the study of Vilagines [7], one or more ports should be created on blades. There are some different structures of the split vane impeller. In this paper, the

structure of modified impeller is based on the normal impeller and the two-dimensional flow theory is used for its hydraulic design. The port is created by cutting off a small part from the blade. The position and axial width of the small port are the two important factors that affect the pump performance. The numerical simulation results of normal impeller in different inlet GVF conditions show that gas mainly concentrates on suction side of the blade on the central area of the impeller while liquid gathers on the pressure side. Therefore, a small flow passage is created at the middle part of the blade in axial direction. To form a channel and make the liquid on pressure side flow into the suction side. Then gas and liquid mix again to effectively reduce the gas gathering area. Fig. 15 shows the three-dimension model of the impeller with split blades. The axial length of impeller is represented by H. The axial width of the small flow channel which is on the middle position of blade is δ. There are serval available values for δ and it maybe relate to the axial length of impeller. In this study, δ is set as 2 mm, It is 4 % of the impeller axial length H, which is also in the range 0-7.5 % recommended by Vilagines [7]. Since the purpose of this study is to evaluate the performance of the split vane impeller on handling high inlet GVFs, different values of δ are not investigated. Optimization of the split vane impeller will be implemented in further study.

The small flow channels on each blades of the impeller make the structure of split vane impeller be more complicated. It is much difficult to create high quality structured mesh. So the unstructured girds were created by ANSYS Workbench Mesh. Fig. 16 shows the mesh of the split vane impeller. The number of elements is 1.98 million and the grid densities near blade edges are all increased. The average element quality is 0.81 which satisfies the grid quality requirement.

Flow characteristics in split vane impeller are also investigated at different inlet GVFs. Fig. 17 shows the gas distribution on different span-wises of the blade-to-blade plane when the inlet GVF is 10 %. It can be seen that there is no high gas volume fraction area in the flow passage. There is not much difference of the gas distribution between the normal impeller and split vane impeller at different span-wise position. Fig. 18 shows the distribution of gas volume fraction in the meridional channel of split vane impeller. It is apparent that the gas volume fraction on split vane impeller is much lower than that of the normal impeller which has been shown before. The highest gas volume fraction on the meridional channel of normal impeller is about 99 %, while the value is just about 14 % on split vane impeller. The gas concentrating area also occurs on the hub near the outlet of split vane impeller, but the gas volume fraction value and gas gathering area are both much smaller than that of the normal impeller.

Gas distribution on the split vane impeller is also investigated at high inlet GVF condition. Fig. 19 shows the variation of gas volume fraction at different span-wises when the inlet GVF is 60 %. At the 10 % span-wise, a small gas gathering area is presented on suction side near the outlet. It gradually decreases from hub to shroud and finally disappears at 90 %

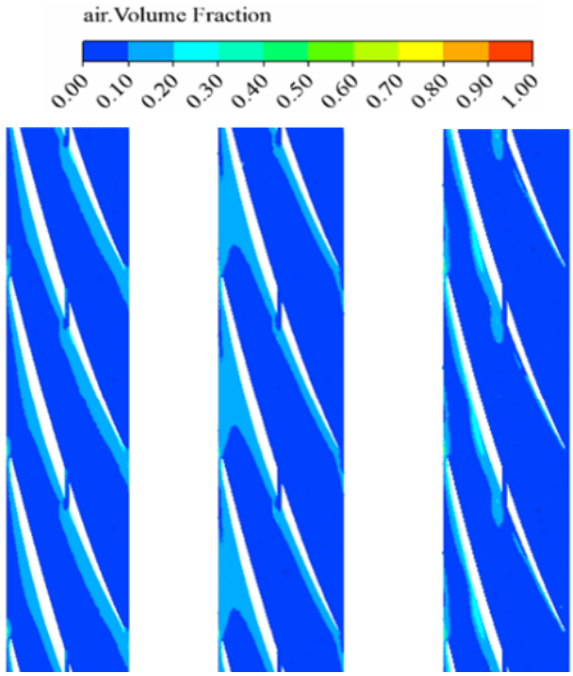

(a) 10 % span-wise (b) 50 % span-wise (c) 90 % span-wise

Fig. 17. Gas distribution at different span-wise (inlet GVF is 10 %).

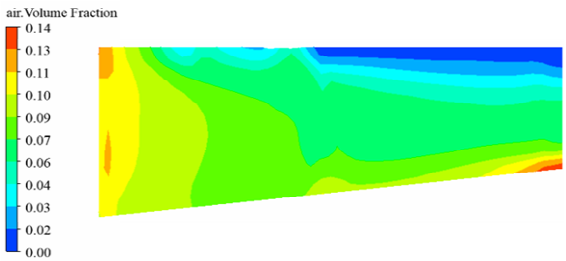

Fig. 18. Gas distribution in meridional channel (inlet GVF is 10 %).

span-wise. Fig. 19(c) shows that gas volume fraction value in the small flow channel on middle position of impeller is almost zero, which means liquid flows from the pressure side of blade to the suction side through the small channel. Fig. 20 shows the gas distribution in the meridional flow channel. The highest gas volume fraction also occurs on hub near the impeller outlet. But the value and the gas concentrating area is much lower than that of the normal impeller. The main reason can be explained from Fig. 21. It shows the distribution of the liquid velocity vectors at 10 % span-wise. Liquid flows through the small channel to the suction side of the blade where gas is mainly accumulating. In this way, liquid and gas mix again in the flow passage. Then the gas pocket area would be dramatically decreased and the pump performance is improved.

The iso-surface gas volume fraction distribution in three-dimensional flow passage of the modified impeller with the inlet GVF 60 % is presented in Fig. 22. The value of the iso-surface GVF is set as 85 % to compare with the normal impel-

Table 2. In-situ gas volume fraction in impeller.

Impeller type	Inlet GVF	
	10 %	60 %
Normal impeller	6.86 %	62.52 %
Split-vane impeller	6.81 %	52.18 %

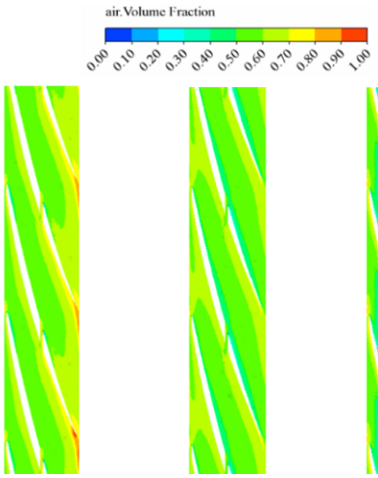

(a) 10 % span wise (b) 50 % span wise (c) 90 % span wise

Fig. 19. Gas distribution at different span-wise (inlet GVF is 60 %).

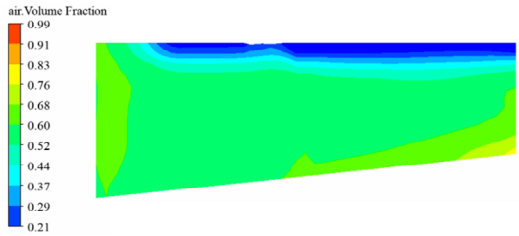

Fig. 20. Gas distribution in meridional flow channel (inlet GVF is 60 %).

ler. The edge of the high gas volume fraction area is located with red closed line in Fig. 22, which just occupies a small area at hub near the outlet of impeller. The value of in-situ gas volume fraction in the normal impeller and split vane impeller are compared at different inlet GVFs [24]. They are shown in Table 2. From Table 2, we can see that the in-situ gas volume fraction in the split impeller are almost the same as that of the normal impeller at low inlet GVF (10 %), while big difference occurs at high inlet GVF (60 %). The in-situ gas volume fraction in split impeller is much lower in high GVFs, which mainly due to the re-mixture of gas and liquid on the suction side of impeller blades.

5.3 Comparison of the performance between normal and modified impellers

The performance of one-stage pump with the split vane impeller and the normal impeller are compared with each other in Fig. 23 at different inlet GVFs ranging from 10 % to 90 %. The flow rate is 100 m^3/h and the rotational speed is 4500 rpm.

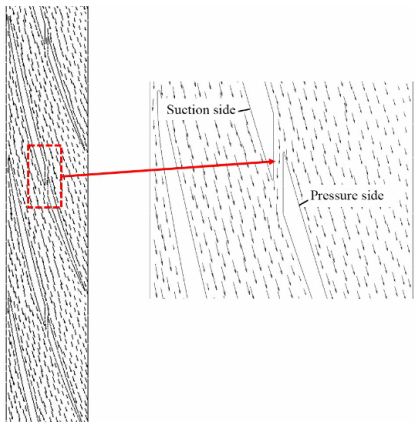

Fig. 21. Distribution of the liquid velocity vectors on blade-to-blade plane (inlet GVF 60 %).

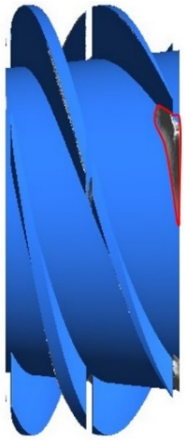

Fig. 22. The iso-surface GVF in the three-dimensional flow passage of modified impeller (inlet GVF is 60 %).

Fig. 23 shows that there is not much difference of the differential pressure between split vane impeller and normal impeller at low and extremely high inlet GVFs. When inlet GVF is 10 %, the differential pressures are 200.45 kPa and 197.95 kPa for split impeller and normal impeller respectively. The improvement of differential pressure in split impeller is not obvious compared with normal impeller at low inlet GVFs. Fig. 24 shows the pressure distribution along the streamwise location in split vane impeller and normal impeller when inlet GVF is 10 %. It indicates that the pressure increment in split impeller is a little higher than normal impeller as well as the total pressure increment of the one compression unit. In Fig. 23, while the inlet GVF is as high as 90 %, the gas-liquid flow can be considered as pure gas. So the effect of small flow channel in spit vane impeller is not obvious and there is no difference on handling very high inlet GVF compared with the normal impeller. Besides the extreme conditions, the differential pressure of split impeller is larger than that of the normal impeller. It is about 12.3 kPa higher than that of the normal impeller when the inlet GVF is 70 %, which is the maximum difference between the two impellers. As the inlet GVF increases,

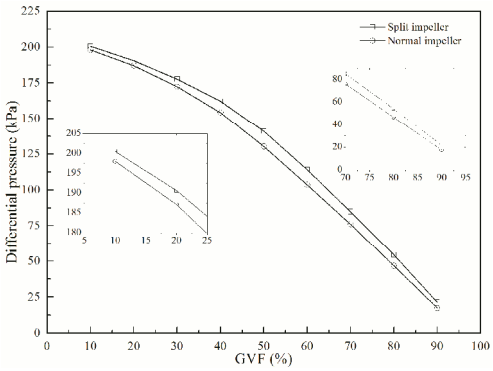

Fig. 23. Differential pressure of the normal and modified impellers.

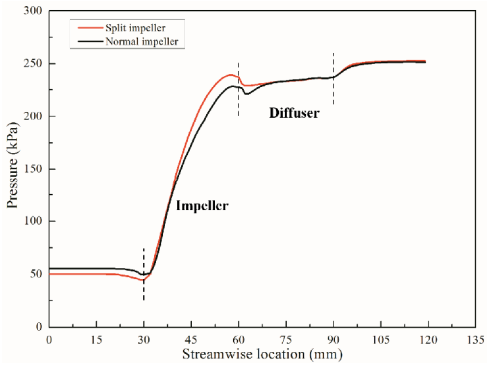

Fig. 24. Pressure distribution along the stream-wise location (inlet GVF is 10 %).

the difference of boosting ability between the two impellers decreases.

6. Conclusions

The gas-liquid flow behavior in a normal impeller at different GVFs ranging from 10 % to 90 % are studied by steady numerical simulations. And the characteristics of gas distribution on the blades of impeller are also analyzed by transient numerical simulations. Then a modified impeller with split vanes is developed to improve the impeller performance especially for high inlet GVF conditions. Gas distribution in the flow field of the modified impeller at different inlet GVFs are investigated. The boosting capability of modified impeller is compared with that of the normal impeller. Through analysis and discussion, some conclusions are concluded as follows:

(1) Gas mainly gathers at the suction side of blade on impeller hub from the center of blade to the outlet. Gas pocket firstly concentrates on the pressure side of blade and occupies most part of the flow passage. Then it moves to the suction side and finally to the outlet along the suction side from the center area of impeller.

(2) The modified impeller with split vanes can effectively suppress gas accumulation in the flow passage and improve the flow conditions by making separated gas-liquid mix again on the suction side of blade. High gas volume fraction area only occurs in a small part near the outlet of impeller. A large amount of hydraulic loss is avoided and the performance is improved especially at high inlet GVFs.

(3) The comparison between the modified impeller and the normal impeller demonstrates that it is better to choose the modified impeller with split vane at high inlet GVFs such as 50 % and 60 %. While as to low inlet GVFs such as 10 % or extremely high inlet GVFs such as 90 %, both the modified impeller and normal impeller are available.

Nomenclature

ANN : Artificial neural network
CFD : Computational fluid dynamics
DOE : Design of experiment
ESP : Electrical submersible pump
ERT : Electrical resistance tomography
GVF : Inlet gas volume fraction
NSGA-II : Non-dominated sorting genetic algorithm-II
SVIP : Split vane impeller pump
SST : Shear stress transport
ρ : Fluid density
v : Velocity vector
P : Pressure
τ : Stress-strain tensor
g : Gravity acceleration vector
F_i : Interphase force
α_g : Gas volume fraction
α_l : Liquid volume fraction
p_1 : Absolute pressure of pump inlet
p_2 : Absolute pressure in gas pipeline
Q_{g1} : Gas volume rate of pump inlet
Q_{g2} : Gas volume rate in gas pipeline
F_i^D : Drag force per unit volume
F_i^L : Virtual mass force per unit volume
F_i^A : Lift force per unit volume
C_D : Drag coefficient
v_l : Liquid velocity
v_g : Gas velocity
Re : Reynolds number
r_g : Diameter of gas bubble
ρ_l : Liquid density
μ_l : Dynamic viscosity of liquid
C_A : Coefficient of virtual mass force
a_A : Additional mass acceleration vector
C_L : Coefficient of lift force

References

[1] J. Y. Zhang, S. J. Cai and H. W. Zhu, Experimental investigation of the flow at the entrance of a rotodynamic multiphase pump by visualization, *Journal of Petroleum Science and Engineering*, 126 (2015) 254-261.

[2] A. Serena and L. E. Bakken, Flow visualization of unsteady and transient phenomena in a mixed-flow multiphase pump, *Proceedings of ASME Turbomachinery Technical Confer-*

ence and Exposition, Seoul, South Korea (2016).
[3] R. Faustini and F. Kenyery, 3D flow modeling in one helical-axial multiphase pump stage through CFD, *USB-LABCEM* (2007).
[4] J. W. Suh, J. W. Kim and Y. S. Choi, Development of numerical Eulerian-Eulerian models for simulating multiphase pumps, *Journal of Petroleum Science and Engineering*, 162 (2018) 588-601.
[5] J. Y. Zhang, H. W. Zhu and C. Yang, Multi-objective shape optimization of helico-axial multiphase pump impeller based on NSGA-II and ANN, *Energy Conversion and Management*, 52 (2011) 538-546.
[6] J. H. Kim and H. C. Lee, Improvement of hydrodynamic performance of a multiphase pump using design of experiment techniques, *Journal of Fluids Engineering*, 137 (2015) 1-15.
[7] R. Vilagines, C. Bratu and F. Spettel, Multiphase fluid pumping or compression device with blades of tandem design, *US patent 6,149,385* (2000).
[8] A. Serena and L. E. Bakken, Experimental study of the influence of the operating parameters on the performance and capability of a mixed-flow multiphase pump, *Proceedings of ASME Turbomachinery Technical Conference and Exposition*, Seoul, South Korea (2016).
[9] G. Morrison, S. Pirouzpanah and K. Kirland, Performance evaluation of a multiphase electric submersible pump, *Offshore Technology Conference*, Texas, USA (2014).
[10] S. Pirouzpanah, S. R. Gudigopuram and G. Morrison, Two-phase flow characterization in a split vane impeller electrical submersible pump, *Journal of Petroleum Science and Engineering*, 148 (2017) 82-93.
[11] ANSYS Inc., ANSYS academic research, release16, help system, *CFX Documentation*, USA (2015).
[12] M. Rakibuzzaman, K. Kim and S. H. Suh, Numerical and experimental investigation of cavitation flows in a multistage centrifugal pump, *Journal of Mechanical Science and Technology*, 32 (3) (2018) 1071-1078.
[13] E. Marsis, S. Pirouzpanah and G. Morrison, CFD-based design improvement for single-phase and two-phase flows inside an electrical submersible pump, *ASME Fluids Engineering Division Summer Meeting*, Nevada, USA (2013).
[14] Y. Shi, H. W. Zhu and J. Y. Zhang, Investigation of condition parameters in each stage of a three-stage helico-axial multiphase pump via numerical simulation, *The 27th International Ocean and Polar Engineering Conference*, California, USA (2017).
[15] Y. Shi, H. W. Zhu, J. Y. Zhang, J. T. Zhang and J. L. Zhao, Experiment and numerical study of a new generation three-stage multiphase pump, *Journal of Petroleum Science and Engineering*, 169 (2018) 471-484.
[16] Y. Di, K. Ahmed and T. Qian, Numerical investigation of cavitation in twin-screw pumps, *Journal of Mechanical Engineering Science* (2017) 1-18.
[17] M. Diaz, A. Iranzo and D. Cuadra, Numerical simulation of the gas-liquid flow in a laboratory scale bubble column: Influence of bubble size distribution and non-drag forces, *Chemical Engineering Journal*, 139 (2008) 363-379.
[18] S. Noroozi and S. H. Hashemabadi, CFD simulation of inlet design effect on deoiling hydrocyclone separation efficiency, *Chemical Engineering and Technology*, 32 (2009) 1885-1893.
[19] M. V. Tabib and P. Schwarz, Quantifying sub-grid scale (SGS) turbulent dispersion force and its effect using one-equation SGS large Eddy simulation (LES) model in a gas-liquid and a liquid-liquid system, *Chemical Engineering Science*, 66 (2011) 3071-3086.
[20] A. Kendoush, The virtual mass of a rotating sphere in fluids, *Journal of Applied Mechanics*, 72 (2005) 801-802.
[21] M. Mohajerani, M. Mehrvar and F. Ein-Mozaffari, CFD analysis of two-phase turbulent flow in internal airlift reactors, *The Canadian Journal of Chemical Engineering*, 90 (2012) 1612-1631.
[22] C. Bratu, Two-phase pump transient behavior, *SPE Annual Technical Conference and Exhibition. Society of Petroleum Engineers*, Dallas, Texas (1995).
[23] J. Y. Zhang, S. J. Cai and Y. J. Li, Visualization study of gas–liquid two-phase flow patterns inside a three-stage rotodynamic multiphase pump, *Experimental Thermal and Fluid Science*, 160 (2016) 125-138.
[24] J. Zhu and H. Q. Zhang, Mechanistic modeling and numerical simulation of in-situ gas void fraction inside ESP impeller, *Journal of Natural Gas Science and Engineering*, 36 (2016) 144-154.

Yi Shi is currently a Ph.D. candidate in China University of Petroleum Beijing. His research interests include the hydraulic design and multiphase flow study in multiphase pumps.